ACS APPLIED POLYMER MATERIALS

pubs.acs.org/acsapm Article

Photooxidative Polymerization of Pyrrole from Photosystem I Proteins

Joshua M. Passantino, Alessia M. Williams, Marc A. Nabhan, David E. Cliffel, and G. Kane Jennings*

Cite This: ACS Appl. Polym. Mater. 2022, 4, 7852−7858 Read Online

ACCESS | Metrics & More | Article Recommendations | Supporting Information

ABSTRACT: The photosystem I (PSI) protein complex is increasingly being utilized because of its robust photoelectrochemical properties. The oxidative ability of the P_{700} reaction site of the protein is less studied than the reductive capabilities of the F_B reaction site. As shown herein, the oxidation potential of P_{700} is robust enough to initiate an oxidative polymerization of the redox monomer, pyrrole. This manuscript reports the first photoactive and conductive protein−polymer composite using extracted, unmodified PSI protein to perform the polymerization process. The polymerization technique consists of adding a monomer and a dopant to a solution of PSI and illuminating the sample with simulated sunlight. Successful polymerization of pyrrole from PSI is confirmed by the combination of infrared spectroscopy, visual observation, thermogravimetric analysis, contact angle measurements, and conductivity measurements. A stable composite between the protein and polymer is indicated by SDS−PAGE and is further supported by photoelectrochemical properties that are opposite in current and potential from those of PSI alone.

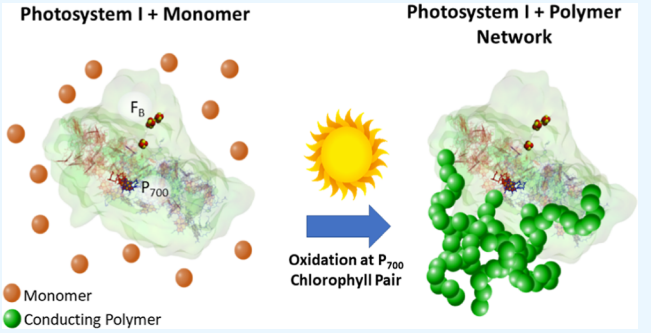

KEYWORDS: *biohybrid, conducting polymer, photopolymerization, photosystem I, polypyrrole, protein−polymer composite*

INTRODUCTION

Protein−polymer composites are a class of biohybrid materials that offer the combination of properties of both synthetic polymers and biomolecules. These composites have been used to advance research in a wide range of fields such as medicine,[1] enzymatic performance,[2] anti-fouling coatings,[3] and catalysis.[4] The fabrication approaches for these composites range from protein encapsulation throughout a bulk polymer to cross-linking proteins to polymer chains.[5] The combination of biomolecules and polymers can lead to biomaterials that are economical, environmentally benign, and highly tunable.

Herein, we present a route for protein−polymer composites in which we use a photoactive redox protein to polymerize an electroactive monomer. The photosystem I (PSI) protein complex is a vital membrane protein of photosynthesis, using the energy from sunlight to transfer electrons across the thylakoid membrane for the ultimate generation of NADH. PSI achieves a nearly perfect quantum yield, driving more than 1 V of potential difference across the thylakoid membrane. PSI has two redox active sites with reduction reactions occurring at the iron−sulfur complex, the F_B site, on the stromal tip of the protein, and oxidations occurring at a special chlorophyll pair, the P_{700} reaction site, located in the lumenal pocket.[6] Many researchers have shown that small redox molecules can be photo-reduced and oxidized at the F_B and P_{700} reaction sites, respectively, of PSI to generate photocurrents on electrodes.[7−13] Here, we show that extracted, unmodified PSI can oxidatively photopolymerize pyrrole to form a photoactive, conductive PSI−polypyrrole composite. Oxidative polymerization by a protein has been shown before. For example, Hira and Payne showed that an iron-containing protein can oxidatively polymerize 3,4-ethylene dioxythiophene (EDOT) in a solution of polystyrene sulfonate (PSS) to form PEDOT:PSS.[14] An innovative aspect of our work herein is that an appropriate electroactive monomer can be *photo-oxidatively polymerized* by a photoactive redox protein.

Research on the integration of PSI with other materials has mostly focused on improving the photoelectrochemical performance of electrodes,[12,13,15−17] as well as producing hydrogen.[18−20] The iron-containing protein complex has been interfaced with conducting polymers in multiple ways, including mixing PSI in a redox polymer,[21] entrapping it in a film during electropolymerization of a monomer,[22] depositing protein and polymer layer-by-layer,[23] and growing a conducting polymer within a PSI film by a vapor-phase process.[24] A common constraint for PSI−polymer systems is the dependence on mediated electron transfer to small redox species

Received: August 11, 2022
Accepted: August 18, 2022
Published: August 31, 2022

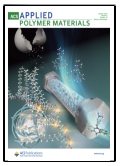

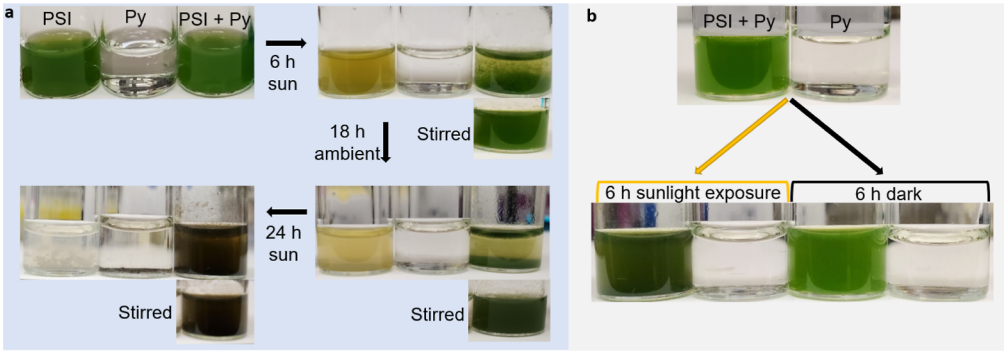

Figure 1. (a) Changes in visual solution properties over time after illumination. From left to right: PSI, Py monomer, PSI + Py monomer. (b) Comparison of visible solution changes after 6 h of illumination or no light.

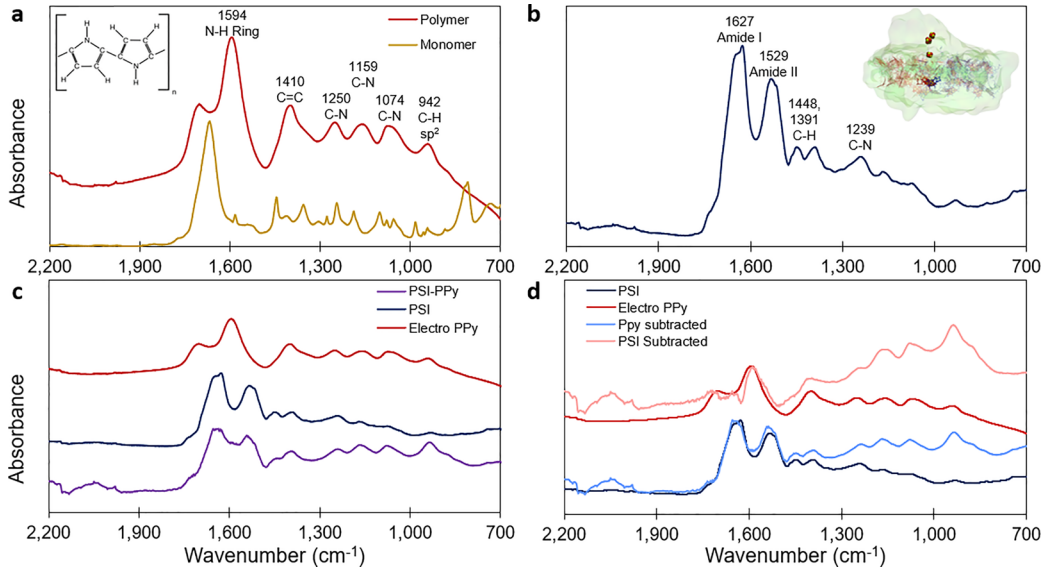

Figure 2. (a) FTIR spectra of Py and electropolymerized PPy film along with characteristic peaks, (b) PSI spectra and characteristic peaks, (c) comparison of PPy grown by PSI to pure PPy and PSI spectra, and (d) result of spectral subtraction of pure components from the reaction product compared to the pure component.

because of a lack of direct connection of the polymer to the active sites for direct electron transfer.[25−27] To achieve a more direct connection, protein conjugates have been formed by other groups using a modified protein complex with a molecular wire connected to a catalyst or enzyme at the F_B site for applications such as hydrogen production.[19,28] Such protein modifications can amplify the cost and processing time for producing these biohybrid materials. In most of this research, there has been a focus on the overall photoelectrochemical redox capabilities of PSI or the robust reductive capability of the F_B site.

The oxidative capabilities of the P_{700} site are also robust, and the P_{700} site has potentials favorable to perform oxidative polymerizations (300 mV vs Ag/AgCl),[29] such as with Py, as we describe here. This process is able to achieve composites of Ppy and PSI that are capable of photoelectrochemistry and photo-enhanced conductivity. This polymerization technique is the first reported conductive, photoactive protein−polymer composite where the polymer is formed by an unmodified protein. This technique could be expanded by using other monomers to tailor the composite functionality as well as other photoactive proteins. The ability to create protein−polymer composites to combine the photo-redox properties of PSI with special properties of the polymer should facilitate the generation of inexpensive, biohybrid solar conversion technology.

RESULTS AND DISCUSSION

Visual Properties. The initial evidence of successful polymerization of Py by PSI proteins was visual. The addition of Py monomer with $NaClO_4$ as an anionic dopant to a dispersion of PSI followed by subsequent illumination of solar light leads to the formation of dark green (characteristic color of PPy)[30] aggregates that eventually precipitate to the bottom of the solution (Figure 1a). The aggregates become increasingly darker with additional light exposure, and a darker green solid approaches black in color after 30 h of solar illumination. As controls, when exposed to simulated sunlight, Py (alone) does not visibly change, and a PSI protein solution becomes bleached by the UV radiation in the solar simulated light. The polymerization also occurs in white light. $NaClO_4$ was selected as a dopant for the polymer because of the large anionic size, compared to other simple anions, and its lack of reactivity with Py as compared to some other dopants that act as chemical oxidizers. The purpose of the dopant is to facilitate

https://doi.org/10.1021/acsapm.2c01404
ACS Appl. Polym. Mater. 2022, 4, 7852−7858

polymerization and increase conductivity by distributing charge throughout the polymer.

To confirm this was a light-dependent reaction, the same experiment was carried out by illuminating monomer and PSI−monomer solutions for 6 h whereas another set of monomer and PSI−monomer solutions was left in the dark (Figure 1b). The illuminated PSI−monomer solution yielded the darker green aggregates, whereas the solutions in the dark remained the same color as under the initial conditions. Red light also triggered the formation of these aggregates, but the solution exposed to the broad-spectrum light yielded dark green aggregates significantly faster than the solution exposed to red light.

Spectroscopic Characterization. ATR-FTIR analysis was used to identify the composition of the products formed upon illumination of PSI with Py monomer (Figure 2). After illumination in broad-spectrum light, the solution was dialyzed to remove unreacted Py, drop-cast onto a gold surface, rinsed with water and then analyzed by FTIR. Figure 2a shows the characteristic spectra for a film of pure electropolymerized PPy with significant peaks at 1594 (N−H bending), 1462 (C═C aromatic stretching), 1250 (C−N stretching), 1159 (C−N stretching), 1074 (C−N stretching), and 942 (C−H sp^2 bending) cm^{-1} that are broader and distinct from those peaks of the Py monomer. Figure 2b shows the spectra of pure PSI with peaks at 1627 (amide I), 1529 (amide II), 1448 (C−H bending), 1391 (C−H bending), and 1239 (C−N stretching) cm^{-1}. Figure 2c shows the spectra for the reaction product obtained by mixing PSI with monomer and illuminating for 3 h. Most notably, the spectra for the reaction product show similar peaks for both PPy (peaks below 1300) and PSI (amide I and II peaks). Additionally, the valley between the amide I and II peaks is higher than that for the pure spectrum, suggesting growth of an aromatic N−H peak as in the PPy spectra.

To compare the reaction product spectra to the two pure components, each spectrum of the pure components was subtracted from the spectrum of the reaction product (Figure 2d). After subtraction of the pure components, the characteristic peaks for both PSI and PPy can be seen in the resultant spectra. The PPy characteristic peaks at 1594, 1462, 1250, 1159, 1074, and 942 cm^{-1} are all prominent in the PSI-subtracted spectrum, and there is no evidence of the monomer peaks at 1663 (C═C stretching) cm^{-1} and 808 (C−H bending) after spectral subtraction, indicating the successful synthesis of PPy that is compositionally consistent with an electropolymerized PPy film. The characteristic peaks for PSI appear at 1627, 1529, 1448, 1391, and 1239 cm^{-1} and are all prominent in the PPy-subtracted spectra with no peak shifting or change in peak shape, suggesting that PSI is still present in the product without degradation.[31]

Our hypothesis is that polymerization of Py is the result of the photooxidative properties of the P_{700} reaction center of PSI. As verification, a solution of chlorophyll a (Chl a) at a concentration similar to that affixed to PSI in solution was exposed to Py and $NaClO_4$ as dopant and irradiated with solar simulated light for 6 h. The PSI control exposed to the same solution produced Ppy based on IR peaks similar to those shown in Figure 2 whereas Chl a did not produce Ppy (Figure S1). Thus, the protein's photooxidative properties are essential to the polymer formation. Figure 3 shows a schematic of the proposed polymerization mechanism in which the P_{700} reaction center photooxidizes Py and oligomers to initiate and propagate the polymerization process.

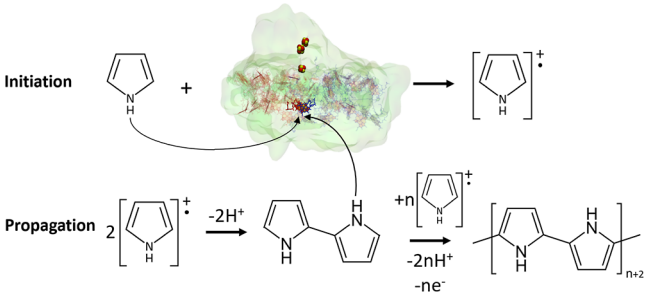

Figure 3. Proposed mechanism for the photooxidative polymerization of Py by the P_{700} reaction center of PSI.

Contact angles of films of pure PSI, pure PPy, and the PSI−PPy reaction product were measured on gold substrates to examine surface property changes. The solutions were dialyzed to remove excess monomer before being drop-cast, and the films were rinsed in distilled water to remove any excess buffer and monomer, leaving only protein and polymer. The contact angles show a significant decrease from 44 ± 3° for the PSI films to 26 ± 7° for the PSI−PPy films whereas pure PPy films exhibit a lower contact angle of 21 ± 7°. The decrease in contact angle for the PSI−PPy films is consistent with a surface that contains both PSI and PPy, supporting the successful polymerization of Py by PSI.

SEM morphologies of powders of traditionally grown PPy and the PSI−monomer reaction product are shown in Figure 4. The chemically synthesized PPy from the addition of ferrocyanide as an oxidant shows a commonly reported morphology of PPy nanoparticles that are coalesced to make a large, networked structure.[32−34] PPy electropolymerized on a gold-coated surface shows similar morphology with connected spherical nanoparticles (Figure S2). The PSI−PPy powder shows a different morphology of solid platelet-like structures instead of a connected nanoparticle network. The formation of PPy platelets has been reported and is most commonly the result of polymerization that is kinetically slower than the more rapid oxidation with ferrocyanide or that by an applied potential on an electrode.[35−37] Additionally, other experiments have shown that longer polymerization times lead to larger nanoparticles with lower definition between each particle.[38] Successful doping of the polymer with perchlorate ions is confirmed by the presence of Cl in EDS spectra (Figure S3).

Properties of PSI−Ppy Composites. The insolubility of Ppy and dialyzed PSI in not only water but also other solvents precludes the use of many common techniques to probe the chemical nature of the protein−polymer composite.[39] As an example, sodium dodecyl sulfate−polyacrylamide gel electrophoresis (SDS−PAGE) shows that PSI is entrapped securely in the composite, as neither the protein nor polymer enters the gel, whereas protein that was physically mixed with pre-synthesized Ppy shows bands consistent with PSI subunits (Figure S4). That the SDS cannot break apart PSI and Ppy interactions suggests strong physical or chemical interactions between the protein and formed polymer.

Thermal properties of the PSI−PPy product were compared to pure PSI films by thermogravimetric analysis (TGA). Figure 5 shows the TGA curves for PSI, PPy, and PSI−PPy after holding at 100 °C for 30 min to evaporate residual water or

https://doi.org/10.1021/acsapm.2c01404
ACS Appl. Polym. Mater. 2022, 4, 7852−7858

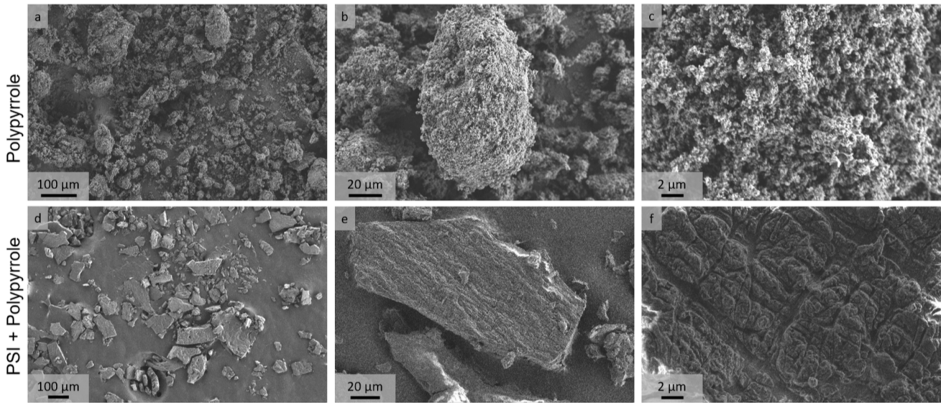

Figure 4. SEM images of PPy (a–c) and PSI–PPy powders (d–f). Magnification increases from left to right.

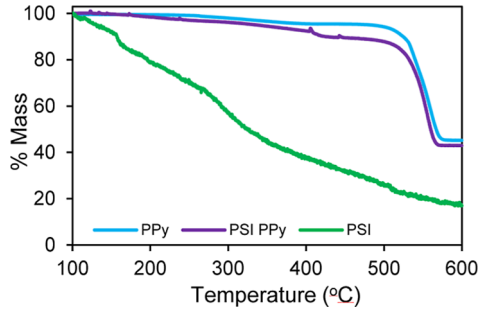

Figure 5. TGA curves of PPy, PSI, and the PSI–PPy reaction product. Samples were held at 100 °C for 30 min before 10 °C/min ramp to 600 °C. The mass of the samples after the 30 min temperature hold was 0.5, 8.7, and 8.5 mg for PSI, PPy, and PSI–PPy, respectively.

monomer. The PPy and PSI–PPy samples lose mass at a slower rate than that of PSI alone until 520 °C where PPy begins to burn off. The similarity between the PPy and PSI–PPy curves further supports the successful polymerization of PPy by PSI. The PSI–PPy sample exhibits far more robust thermal properties as compared to PSI alone. This trend holds true if the PPy contribution is subtracted from PSI–PPy to compare only the PSI contributions to the thermal properties (Figure S5).

Electrochemical properties of the protein–polymer composite were investigated by measuring the photopotential and photocurrent of the cast films in an ascorbate (AscH):2,6-dichlorophenolindophenol (DCPIP) redox mediator system and comparing them to unmodified PSI films. Figure 6a shows the average open-circuit potential (OCP) of seven independently prepared PSI and PSI–PPy multilayer films deposited on gold, as well as the photopotential response of PSI deposited atop a PPy film polymerized on gold via an applied potential. Figure 6b shows the comparison of the magnitude of the photopotential change by normalizing the potential at 20 s to 0 V. Figure 6c shows the comparison of photocurrents.

A PSI film on bare gold shows a dark OCP of around −59 mV, which is increased by 10 mV after 30 s of illumination. The redox potential of PPy is known to be −200 mV vs Ag/AgCl;[40] therefore, PPy deposited onto a gold substrate should lower the potential. Both bare gold and an independently electropolymerized PPy film show no photoactivity (Figure S6), so any change in Figure 6 results from the redox properties of the protein. The PSI–PPy reaction product has a dark OCP of −110 mV, and the potential decreases by 10 mV

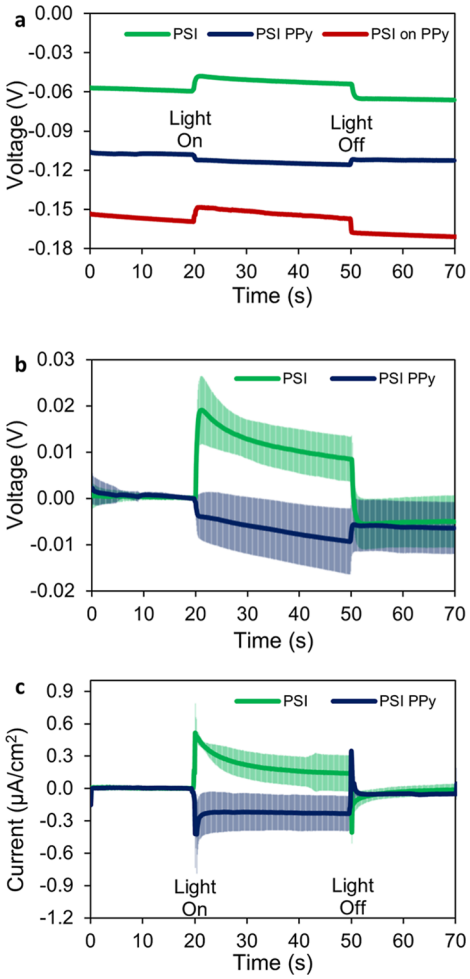

Figure 6. OCP response to photo-illumination of films on gold in a 1:20 mM AscH:DCPIP mediator. Illumination begins at 20 s and ends at 50 s and potentials are vs Ag/AgCl. Shaded regions are indicative of standard deviation over seven samples. (a) Potential response for pure PSI, PSI–monomer reaction product, and PSI deposited on a PPy film, (b) OCP's normalized to 0 V for response magnitude comparison, and (c) photocurrent response for PSI and PSI–PPy films held at the dark OCP.

after 30 s of illumination, the opposite potential change of PSI alone. A decrease in photopotential indicates that there is an increase in the ratio of reduced to oxidized species near the electrode and an increase indicates the opposite. If the P_{700}

https://doi.org/10.1021/acsapm.2c01404
ACS Appl. Polym. Mater. 2022, 4, 7852–7858

reaction center of the PSI protein is reduced directly by electrons flowing from the electrode through Ppy, then the composite film is able to more readily generate reduced species to elevate this ratio and decrease the photopotential.

The photocurrent trends mirror the photopotential trends where PSI generates 0.14 $\mu A/cm^2$ of cathodic current and PSI−PPy generates 0.23 $\mu A/cm^2$ of anodic current. This cathodic photocurrent for PSI alone in the AscH:DCPIP couple has been attributed to the fast oxidation of $DCPIPH_2$ at the P_{700} site of PSI to yield an excess of oxidized species that are readily reduced at the electrode.[16] An anodic photocurrent for PSI−PPy suggests that the presence of the polymer alters the relative redox kinetics at the PSI active sites to increase the ratio of reduced to oxidized species.

To investigate the connection between the protein and polymer, PSI was deposited on top of an independently grown PPy film. This film has a lower dark OCP of −156 mV because of the presence of pure PPy on the electrode, but the potential increases upon illumination, showing the same trend as PSI on bare gold. Drop-casting PSI on top of a PPy film does not result in direct interactions between the polymer and the P_{700} active site of the protein, so the electrochemical properties of PSI remain the same as PSI on a metal electrode. This important control further supports direct interactions between the polymer and protein in the PSI−PPy composite because of the opposite photoelectrochemical capabilities as compared to PSI alone.

PPy is an intrinsically conducting material, and if sufficient polymer is grown and connected to photoactive PSI, then the resulting product should be a photoactive and conductive composite. The conductivity of PPy and PSI−PPy reaction product powders was measured by compressing the powders between two metal electrodes (see Figure S7). The conductivity was calculated using the following equation

$$\kappa = \frac{h}{R \cdot A} \quad (1)$$

where κ = electrical conductivity (S/cm), h = powder height (cm), R = electrical resistance (Ω), and A = cross-sectional area of powder (cm^2).[41] For simplicity of measurement and because of the non-uniformity of particle sizes as shown in the SEM images, the pellets were assumed to have no porosity due to the compressive force, which artificially lowers the measured conductivities.

The conductivity for pure PPy was measured to be $2.3 \times 10^{-4} \pm 1.4 \times 10^{-4}$ S/cm, similar to other PPy powder conductivities in the literature, and the value was the same in the light or in the dark.[42] If the PSI−PPy powder is photoactive, then there should be a difference in conductivity when measured in darkess and under illumination. In the dark, the conductivity was $1.93 \times 10^{-5} \pm 7.5 \times 10^{-8}$ S/cm and in the light it was $3.09 \times 10^{-5} \pm 1.8 \times 10^{-6}$ S/cm, a 60% increase in conductivity upon illumination. Due to the constraints of the testing apparatus, the powders were illuminated only from the side, leaving the majority of the cross sections of the pellets in the dark, so the conductivity of the PSI−PPy powder should be even higher under more complete illumination. The order of magnitude decrease in conductivity compared to the pure PPy is likely due to the insulating properties of the non-electron conducting portions of PSI. The conductivity measurements confirm that the conducting polymer was grown and is interfaced with the PSI protein to form a photoactive, conducting composite.

CONCLUSIONS

Pyrrole was successfully polymerized using the photooxidative properties of PSI to form a photoactive and conductive PSI−PPy composite. The polymerization occurs by mixing PSI with both the Py monomer and a dopant and then illuminating the solution to initiate the polymerization process. Growth of PPy was confirmed by comparing the reaction product to both PSI and independently polymerized samples through FTIR, TGA, and contact angle measurements. TGA showed that the PSI−PPy composite is more thermally robust than PSI alone and acts similarly to pristine PPy. SEM images showed a platelet-like morphology for the PSI−PPy particles and coalesced nanoparticle morphology for electrochemically and chemically grown polymer. Successful entrapment of PSI within the grown PPy is supported by SDS−PAGE results showing that protein within the composite does not migrate into the gel as compared to protein that was mixed with the pre-synthesized polymer. Additionally, the PSI−PPy composite alters the photoelectrochemical properties as compared to pure PSI, suggesting that the connected polymer can transfer electrons directly to or from an electrode to the protein's P_{700} site. The composite was also measured to be conductive and photoactive in solid-state systems, proving that conducting PPy was grown and is well-connected to the PSI proteins.

This manuscript is the first report of polymerization by PSI to form a protein−polymer composite. The resulting material is both conductive and photoactive, enabling use in both liquid- and solid-state solar conversion processes. Integrating PSI into solid-state systems is notoriously difficult because of connectivity issues between the protein and conducting polymers, and the PSI−PPy composite can greatly mitigate this issue. The capability of PSI to perform an oxidative polymerization can be expanded to grow different polymers to obtain new classes of protein−polymer composites with unique photoelectrochemical properties through facile synthesis methods.

MATERIALS AND METHODS

PSI Extraction. PSI was extracted from locally purchased spinach following a procedure described in a previous work.[43] In short, the spinach was deveined, macerated, filtered, and then centrifuged at 8000*g* to isolate the thylakoid membranes. The supernatant was then mixed with a surfactant (TritonX-100) to lyse the membranes before a second centrifugation at 20,000*g*. A hydroxyapatite column was used to isolate the PSI. The protein was dialyzed in a 1 to 4000 volume ratio of deionized water for 24 h using a 10,000 MWCO dialysis tubing to remove salts and surfactants.

Photopolymerization. Photopolymerization was carried out by adding pyrrole monomer (Sigma-Aldrich) into a solution of ∼4 μM PSI and 1.0 M $NaClO_4$ to a concentration of 0.5 M pyrrole and mixing with an ultrasonicator until all pyrrole was solubilized. The mixture was then illuminated using a Newport xenon arc lamp solar simulator, which emitted a light intensity of 330 mW/cm^2. Illumination times varied from 3 to 24 h, depending on the sample. Every sample was dialyzed to remove unreacted monomer and excess salt before characterization.

Characterization Methods. FTIR measurements were taken with a Nicolet 6700 FTIR at 4 cm^{-1} resolution. To prepare samples for FTIR, solutions were first dialyzed to remove excess monomer and salt, drop-casted onto a gold surface, and rinsed in water before measurements. Spectral subtraction was performed using OMNIC Specta software. Samples for contact angle measurements were made in the same manner and were measured with deionized water using a manual Rame-Hart goniometer. SEM measurements were taken with a Zeiss Merlin scanning electron microscope with an accelerating

https://doi.org/10.1021/acsapm.2c01404
ACS Appl. Polym. Mater. 2022, 4, 7852−7858

voltage of 2.00 kV. Samples were filtered through a 0.45 μM filter, rinsed with water, and dried to form a powder that was imaged on a gold substrate.

SDS−PAGE was performed on samples that were exposed to illumination for 6 h. The samples were then concentrated in a 10K MWCO Pierce concentrator. After concentration, the samples were prepared as recommended by Invitrogen guidelines using a NuPAGE 10% Bis-Tris Gel.

For TGA measurements, samples were dialyzed and concentrated after reaction in light and then 200 μL of the resulting solution was vacuum-dried in a ceramic sample pan. The pan was then placed in an STA-i 1000 thermogravimetric analyzer, and air was flowed through the furnace. Samples were heated to 100 °C at a rate of 10 °C/min and held for 30 min before a 10 °C/min ramp to 600 °C.

Electrochemical characterization was performed using a CH Instruments CH660a workstation equipped with a Faraday cage. Saturated Ag/AgCl was used as the reference electrode with a platinum mesh counter electrode and 1 M KCl was used as the electrolyte. Samples were drop-cast onto gold-coated silicon substrates for measurements. Photopotential and photocurrent were measured by 30 s of illumination using a 250 W cold light source (Leica KL 2500 LCD), which emitted a light intensity of 80 mW/cm^2 at a spectral range of 380−790 nm.

Conductivity was measured using a two-electrode experimental setup (Figure S7) connected to a Gamry Reference 600 potentiostat. The setup consists of a transparent glass tube with two stainless-steel rods that fit snugly in the tube. Powder was placed between the rods and an external force of 300 N was applied to the top electrode to compress the powder. Samples were illuminated on one side of the tube using the same lamp as was used in the electrochemical measurements. The resistance across the powder and the compressed powder height were measured to use in eq 1 to calculate conductivity.

■ ASSOCIATED CONTENT

Supporting Information

The Supporting Information is available free of charge at https://pubs.acs.org/doi/10.1021/acsapm.2c01404.

IR spectra showing an absence of Ppy growth with chlorophyll a, SEM image of electrochemically synthesized PPy, EDS maps showing successful doping, SDS−PAGE analysis, normalized TGA curves to compare PSI thermal stability, photoactivity comparison with gold and pure PPy film, and powder conductivity experimental setup (PDF)

■ AUTHOR INFORMATION

Corresponding Author

G. Kane Jennings − *Department of Chemical and Biomolecular Engineering, Vanderbilt University, Nashville, Tennessee 37235, United States;* orcid.org/0000-0002-3531-7388; Email: kane.g.jennings@vanderbilt.edu

Authors

Joshua M. Passantino − *Department of Chemical and Biomolecular Engineering, Vanderbilt University, Nashville, Tennessee 37235, United States;* orcid.org/0000-0002-4707-6016

Alessia M. Williams − *Department of Chemical and Biomolecular Engineering, Vanderbilt University, Nashville, Tennessee 37235, United States*

Marc A. Nabhan − *Department of Chemical and Biomolecular Engineering, Vanderbilt University, Nashville, Tennessee 37235, United States*

David E. Cliffel − *Department of Chemistry, Vanderbilt University, Nashville, Tennessee 37235, United States;* orcid.org/0000-0001-8756-106X

Complete contact information is available at: https://pubs.acs.org/10.1021/acsapm.2c01404

Author Contributions

The manuscript was written through contributions of all authors. All authors have given approval to the final version of the manuscript.

Funding

We gratefully acknowledge support from the U.S. Department of Agriculture (2019-67021-29857) for providing funding that was used by all authors of this manuscript. Author 1 received funding from the NSF Graduate Research Fellowship Program (DGE-1445197 and DGE-1937963). Author 2 received funding from the National Science Foundation-Research Experiences for Undergraduates (DMR-1852157) awarded to the Vanderbilt Institute of Nanoscale Science and Engineering.

Notes

The authors declare no competing financial interest.

■ ACKNOWLEDGMENTS

We acknowledge support from the Vanderbilt Institute of Nanoscale Science and Engineering (VINSE) for the use of their characterization tools and technical support. We thank Dr. Blaise Kimmel for insightful discussions.

■ ABBREVIATIONS

PSI	photosystem I
Py	pyrrole
PPy	polypyrrole
TGA	thermogravimetric analysis
SDS−PAGE	sodium dodecyl sulfate−polyacrylamide gel electrophoresis
ATR-FTIR	attenuated total reflection Fourier transform infrared spectroscopy
OCP	open-circuit potential

■ REFERENCES

(1) Wang, F.; Li, Y.; Gough, C. R.; Liu, Q.; Hu, X. Dual-Crystallizable Silk Fibroin/Poly(L-Lactic Acid) Biocomposite Films: Effect of Polymer Phases on Protein Structures in Protein-Polymer Blends. *Int. J. Mol. Sci.* **2021**, *22*, 1871.

(2) Thiele, M. J.; Davari, M. D.; König, M.; Hofmann, I.; Junker, N. O.; Mirzaei Garakani, T.; Vojcic, L.; Fitter, J.; Schwaneberg, U. Enzyme-Polyelectrolyte Complexes Boost the Catalytic Performance of Enzymes. *ACS Catal.* **2018**, *8*, 10876−10887.

(3) Grover, N.; Plaks, J. G.; Summers, S. R.; Chado, G. R.; Schurr, M. J.; Kaar, J. L. Acylase-Containing Polyurethane Coatings with Anti-Biofilm Activity. *Biotechnol. Bioeng.* **2016**, *113*, 2535−2543.

(4) Li, X.; Cao, Y.; Luo, K.; Sun, Y.; Xiong, J.; Wang, L.; Liu, Z.; Li, J.; Ma, J.; Ge, J.; Xiao, H.; Zare, R. N. Highly Active Enzyme−Metal Nanohybrids Synthesized in Protein−Polymer Conjugates. *Nat. Catal.* **2019**, *2*, 718−725.

(5) Gill, I.; Ballesteros, A. Bioencapsulation within Synthetic Polymers (Part 2): Non-Sol-Gel Protein-Polymer Biocomposites. *Trends Biotechnol.* **2000**, *18*, 469−479.

(6) Nelson, N.; Yocum, C. F. Structure and Function of Photosystems I and II. *Annu. Rev. Plant Biol.* **2006**, *57*, 521−565.

(7) Yu, D.; Wang, M.; Zhu, G.; Ge, B.; Liu, S.; Huang, F. Enhanced Photocurrent Production by Bio-Dyes of Photosynthetic Macromolecules on Designed TiO_2 Film. *Sci. Rep.* **2015**, *5*, 9375.

(8) Frolov, L.; Wilner, O.; Carmeli, C.; Carmeli, I. Fabrication of Oriented Multilayers of Photosystem I Proteins on Solid Surfaces by Auto-Metallization. *Adv. Mater.* **2008**, *20*, 263−266.

(9) Ciesielski, P. N.; Hijazi, F. M.; Scott, A. M.; Faulkner, C. J.; Beard, L.; Emmett, K.; Rosenthal, S. J.; Cliffel, D. E.; Kane Jennings,

G. K. Photosystem I-Based Biohybrid Photoelectrochemical Cells. *Bioresour. Technol.* **2010**, *101*, 3047−3053.
(10) Heifler, O.; Carmeli, C.; Carmeli, I. Enhanced Optoelectronics by Oriented Multilayers of Photosystem I Proteins in Dry Hybrid Bio-Solid Devices. *J. Phys. Chem. C* **2018**, *122*, 11550−11556.
(11) LeBlanc, G.; Gizzie, E. A.; Yang, S.; Cliffel, D. E.; Jennings, G. K. Photosystem I Protein Films at Electrode Surfaces for Solar Energy Conversion. *Langmuir* **2014**, *30*, 10990−11001.
(12) Chen, W.-L.; Gross, E. L.; Pan, R. L. A Photoelectrochemical Cell Using Electrodes Modified by Photosystem I Particles of Spinach. *Bot. Bull. Acad. Sinica* **1992**, *33*, 9−15.
(13) Baker, D. R.; Simmerman, R. F.; Sumner, J. J.; Bruce, B. D.; Lundgren, C. A. Photoelectrochemistry of Photosystem I Bound in Nafion. *Langmuir* **2014**, *30*, 13650−13655.
(14) Hira, S. M.; Payne, C. K. Protein-Mediated Synthesis of the Conducting Polymer PEDOT:PSS. *Synth. Met.* **2013**, *176*, 104−107.
(15) Nguyen, K.; Bruce, B. D. Growing Green Electricity: Progress and Strategies for Use of Photosystem I for Sustainable Photovoltaic Energy Conversion. *Biochim. Biophys. Acta Bioenerg.* **2014**, *1837*, 1553−1566.
(16) Passantino, J. M.; Wolfe, K. D.; Simon, K. T.; Cliffel, D. E.; Jennings, G. K. Photosystem I Enhances the Efficiency of a Natural, Gel-Based Dye-Sensitized Solar Cell. *ACS Appl. Bio Mater.* **2020**, *3*, 4465−4473.
(17) Wolfe, K. D.; Dervishogullari, D.; Stachurski, C. D.; Passantino, J. M.; Jennings, G. K.; Cliffel, D. E. Photosystem I Multilayers within Porous Indium Tin Oxide Cathodes Enhance Mediated Electron Transfer. *Chemelectrochem* **2020**, *7*, 596−603.
(18) LeBlanc, G.; Chen, G.; Jennings, G. K.; Cliffel, D. E. Photoreduction of Catalytic Platinum Particles Using Immobilized Multilayers of Photosystem I. *Langmuir* **2012**, *28*, 7952−7956.
(19) Lubner, C. E.; Grimme, R.; Bryant, D. A.; Golbeck, J. H. Wiring Photosystem I for Direct Solar Hydrogen Production. *Biochemistry* **2010**, *49*, 404−414.
(20) Krassen, H.; Schwarze, A.; Friedrich, B.; Ataka, K.; Lenz, O.; Heberle, J. Photosynthetic Hydrogen Production by a Hybrid Complex of Photosystem I and [NiFe]-Hydrogenase. *ACS Nano* **2009**, *3*, 4055−4061.
(21) Zhao, F.; Conzuelo, F.; Hartmann, V.; Li, H.; Nowaczyk, M. M.; Plumeré, N.; Rögner, M.; Schuhmann, W. Light Induced H2 Evolution from a Biophotocathode Based on Photosystem 1—Pt Nanoparticles Complexes Integrated in Solvated Redox Polymers Films. *J. Phys. Chem. B* **2015**, *119*, 13726−13731.
(22) Gizzie, E. A.; LeBlanc, G.; Jennings, G. K.; Cliffel, D. E. Electrochemical Preparation of Photosystem I-Polyaniline Composite Films for Biohybrid Solar Energy Conversion. *ACS Appl. Mater. Interfaces* **2015**, *7*, 9328−9335.
(23) Wolfe, K. D.; Gargye, A.; Mwambutsa, F.; Than, L.; Cliffel, D. E.; Jennings, G. K. Layer-by-Layer Assembly of Photosystem I and PEDOT:PSS Biohybrid Films for Photocurrent Generation. *Langmuir* **2021**, *37*, 10481−10489.
(24) Robinson, M. T.; Simons, C. E.; Cliffel, D. E.; Jennings, G. K. Photocatalytic Photosystem I/PEDOT Composite Films Prepared by Vapor-Phase Polymerization. *Nanoscale* **2017**, *9*, 6158−6166.
(25) Saboe, P. O.; Conte, E.; Chan, S.; Feroz, H.; Ferlez, B.; Farell, M.; Poyton, M. F.; Sines, I. T.; Yan, H.; Bazan, G. C.; Golbeck, J. H.; Kumar, M. Biomimetic Wiring and Stabilization of Photosynthetic Membrane Proteins with Block Copolymer Interfaces. *J. Mater. Chem. A* **2016**, *4*, 15457−15463.
(26) Gizzie, E. A.; Scott Niezgoda, J.; Robinson, M. T.; Harris, A. G.; Kane Jennings, G. K.; Rosenthal, S. J.; Cliffel, D. E. Photosystem I-Polyaniline/TiO_2 Solid-State Solar Cells: Simple Devices for Biohybrid Solar Energy Conversion. *Energy Environ. Sci.* **2015**, *8*, 3572−3576.
(27) Kazemzadeh, S.; Riazi, G.; Ajeian, R. Novel Approach of Biophotovoltaic Solid State Solar Cells Based on a Multilayer of PS1 Complexes as an Active Layer. *ACS Sustain. Chem. Eng.* **2017**, *5*, 9836−9840.
(28) Grimme, R. A.; Lubner, C. E.; Bryant, D. A.; Golbeck, J. H. Photosystem I/Molecular Wire/Metal Nanoparticle Bioconjugates for the Photocatalytic Production of H2. *Chemtracts* **2008**, *130*, 6308−6309.
(29) Sadki, S.; Schottland, P.; Brodie, N.; Sabouraud, G. The Mechanisms of Pyrrole Electropolymerization. *Chem. Soc. Rev.* **2000**, *29*, 283−293.
(30) Jung, Y.; Spray, R. L.; Kim, J. H.; Kim, J. M.; Choi, K. S. Selective Polymerization of Polypyrrole in Silica Mesopores Using an in Situ Generated Oxidizing Agent on a Silica Surface. *Chem. Commun.* **2010**, *46*, 6566−6568.
(31) Arrondo, J. L. R.; Goñi, F. M. Structure and Dynamics of Membrane Proteins as Studied by Infrared Spectroscopy. *Prog. Biophys. Mol. Biol.* **1999**, *72*, 367−405.
(32) Saoudi, B.; Jammul, N.; Chehimi, M. M.; Jaubert, A. S.; Arkam, C.; Delamar, M. XPS Study of the Adsorption Mechanisms of DNA onto Polypyrrole Particles. *Spectroscopy* **2004**, *18*, 519−535.
(33) Istakova, O. I.; Konev, D. V.; Medvedeva, T. O.; Zolotukhina, E. V.; Vorotyntsev, M. A. Efficiency of Pyrrole Electropolymerization under Various Conditions. *Russ. J. Electrochem.* **2018**, *54*, 1243−1251.
(34) Karami, H.; Nezhad, A. R. Investigation of Pulse-Electropolymerization of Conductive Polypyrrole Nanostructures. *Int. J. Electrochem. Sci.* **2013**, *8*, 8905−8921.
(35) Lima, R. M. A. P.; de Oliveira, M. C. A.; de Oliveira, H. P. Wearable Supercapacitors Based on Graphene Nanoplatelets/Carbon Nanotubes/Polypyrrole Composites on Cotton Yarns Electrodes. *SN Appl. Sci.* **2019**, *1*, 325.
(36) Wang, T.; Zhong, W.; Ning, X.; Wang, Y.; Yang, W. Facile Route to Hierarchical Conducting Polymer Nanostructure: Synthesis of Layered Polypyrrole Network Plates. *J. Appl. Polym. Sci.* **2009**, *114*, 3855−3862.
(37) Shinde, S. S.; Gund, G. S.; Dubal, D. P.; Jambure, S. B.; Lokhande, C. D. Morphological Modulation of Polypyrrole Thin Films through Oxidizing Agents and Their Concurrent Effect on Supercapacitor Performance. *Electrochim. Acta* **2014**, *119*, 1−10.
(38) Chen, X.; Issi, J.; Devaux, J. P.; Billaud, D. Chemically Oxidized Polypyrrole: Influence of the Experimental Conditions on Its Electrical Conductivity and Morphology. *Polym. Eng. Sci.* **1995**, *35*, 642−647.
(39) Frommer, J. E. Conducting Polymer Solutions. *Acc. Chem. Res.* **1986**, *19*, 2−9.
(40) Street, G. B.; Clarke, T. C.; Geiss, R. H.; Lee, V. Y.; Nazzal, A.; Pfluger, P.; Scott, J. C. Characterization of Polypyrrole. *J. Phys. Colloq.* **1983**, *44*, C3-599−C3-606.
(41) Hoffmann, V.; Rodriguez Correa, C.; Sautter, D.; Maringolo, E.; Kruse, A. Study of the Electrical Conductivity of Biobased Carbonaceous Powder Materials under Moderate Pressure for the Application as Electrode Materials in Energy Storage Technologies. *GCB Bioenergy* **2019**, *11*, 230−248.
(42) Håkansson, E.; Lin, T.; Wang, H.; Kaynak, A. The Effects of Dye Dopants on the Conductivity and Optical Absorption Properties of Polypyrrole. *Synth. Met.* **2006**, *156*, 1194−1202.
(43) Reeves, S. G.; Hall, D. O. Higher Plant Chloroplasts and Grana: General Preparative Procedures (Excluding High Carbon Dioxide Fixation Ability Chloroplasts). *Methods Enzymol.* **1980**, *69*, 85−94.

https://doi.org/10.1021/acsapm.2c01404
ACS Appl. Polym. Mater. 2022, 4, 7852−7858